

1 **Response to Reviewer comments by Nadav Wetzler:**

2 Thank you for your time in reviewing our paper. Below is our response to your comments and description of the
3 modifications we made to address them.

4 *I would expect a more deterministic approach to validate the resulted faults geometry. I think that exploring a small region*
5 *using FMS data + mapped fault will be much appreciated to judge, is method is more capable to detect the natural faults*
6 *network?*

7 We agree with the sentiment that focal mechanism solutions (FMS) can reveal important information regarding the geometry
8 of the faults under investigation. Deterministic measures that investigate the compatibility between reconstructed faults and
9 the focal mechanisms of the events have been introduced and extensively studied by our group in research by Wang et al
10 2013. The FMS are greatly dependent on the location and the velocity model used for the inversions. Thus it would be
11 inconsistent to use the solutions obtained using cross-correlation based relative locations with our absolute location catalog
12 obtained using a different velocity model. That is why we focused on validations based on information criteria and cross
13 correlation.

14 In an effort to address your comment we updated Figure 5 (now Figure 6) by adding the fault trace of the Landers fault as
15 obtained from the Community Fault Model of southern California. We also added the following text to inform the reader
16 about FMS based validation approaches.

17 *“It is also possible to employ metrics based on consistency of focal mechanism solutions to evaluate the reconstructed faults.*
18 *For a detailed application of such metrics the reader is referred to the detailed work by Wang et al.(2013). In this study,*
19 *since we do not have focal mechanism solutions for our target catalog, we focus on information criteria metrics and out of*
20 *sample forecast tests.”*

21 *Specific comments: L. 33: The use of “large durations” is confusing. Please clarify. Fig. 10: It seems that the colors of the*
22 *ellipses is correlated with the size of the kernel. If so, a color bar is useful here.*

23 We have clarified the term to express catalogs covering long time spans. In Figure 10 (now Figure 11) have added a color
24 bar and also supplemented the figure caption to indicate that the color axis unit.

25 *“Clusters are colored according their density (data point per km³) where the volume is estimated as the product of standard*
26 *deviations along the principal component axes.”*

27 **References:**

28
29 Wang, Y., G. Ouillon, J. Woessner, D. Sornette, and S. Husen (2013), Automatic reconstruction of fault networks from
30 seismicity catalogs including location uncertainty, *J. Geophys. Res. Solid Earth*, 118(11), 5956–5975,
31 doi:10.1002/2013JB010164.

32

33

34

35 **Response to Reviewer comments by Leandro C. Gallo:**

36 Thank you for taking the time to review our paper and providing detailed suggestions. Below is our response to your
37 comments and description of the modifications we made to address them.

38 *Its application to a single synthetic experiment is practical for making the whole workflow understood, however, it has no*
39 *statistical significance in terms of method's sensitivity. Being that the synthetic experiment features a relatively small*
40 *number of data points, I would rather advise the authors to apply the technique to a larger number of models featuring a*
41 *different number of faults with diverse characteristics or orientations –without prior knowledge this would be*
42 *computationally inexpensive. Assessing discrepancies between the true and the inferred plane segments in a number large*
43 *enough would then allow statistically meaningful results that, in my opinion, would make the whole manuscript more robust.*

44 We agree with you that the synthetics provided previously did not allow for conclusions about the sensitivity and robustness
45 of the method. We have therefore supplemented the synthetics section with a more elaborate study where we gradually
46 increase the sampling of a ground truth fault network under different background noise levels and investigate the method's
47 clustering performance using the Rand index. This is now covered in section 3.1 and the results are provided in Figure 5.

48 L. 52: The contribution of source code to this section as supplementary materials –or open-access code repositories like
49 GitHub or Zenodo- would boost scientific progress and reproducibility.

50 Based on your suggestions we have made publicly available the codes for the agglomerative clustering and the codes for the
51 generation and evaluation of the synthetic sensitivity analysis. The links are included in the “Code availability” section.

52 L. 53: I don't see this subsection appropriate for the “methods” section.

53 We have moved this part to a separate section after the introduction.

54 L.86-88: The criterion applied for merging two clusters involves the minimum squared Euclidean distances, was this
55 criterion chosen for any particular reason? Is there any other metric to use instead for clustering? I'm thinking about the
56 Eigen-based parameters of the covariance matrix. It would be valuable some extra explanation.

57 Our selection of the Ward's criterion was motivated by its characteristic of producing regular sized clusters. This is
58 important for the atomization procedure because we want all clusters to have the same potential to merge and grow into
59 bigger structures. Initially we also investigated using the Mahalanobis distance with single linkage, and using the Gaussian
60 associated with the location uncertainty of each event without atomization. These methods were not successful in
61 reconstructing the synthetic networks in the presence of background noise; hence we focused our attention on atomization
62 using the Ward creation. We have added the following sentence to the method section.

63 *“While there are many different linkage methods and distance metrics, here we have chosen to use the Ward's criterion*
64 *because it produces clusters with regular sizes. This is important for the atomization procedure as we want clusters to have*
65 *similar potentials to merge and grow into bigger structures.”*

66
67 L.110, Figure 2: for those who are unfamiliar with the method, the hierarchical, binary cluster tree is most easily understood
68 when viewed graphically. It would be helpful for the understanding of those who are not familiar to add the associated
69 dendrogram to this figure.

70 We have added the dendrograms for both datasets to Figure 2.

Fault Network Reconstruction using Agglomerative Clustering: Applications to South Californian Seismicity

Yavor Kamer^{1,a}, Guy Ouillon², Didier Sornette¹

¹ETH Zurich, Switzerland

²Lithophyse, Nice, France

^anow at: RichterX.com

Correspondence to: Yavor Kamer (yaver.kamer@gmail.com)

Abstract

In this paper we introduce a method for fault network reconstruction based on the 3D spatial distribution of seismicity. One of the major drawbacks of statistical earthquake models is their inability to account for the highly anisotropic distribution of seismicity. Fault reconstruction has been proposed as a pattern recognition method aiming to extract this structural information from seismicity catalogs. Current methods start from simple large scale models and gradually increase the complexity trying to explain the small scale features. In contrast the method introduced here uses a bottom-up ~~that~~ **approach**, ~~that~~ **re**lies on initial sampling of the small scale features and reduction of this complexity by optimal local merging of substructures.

First, we describe the implementation of the method through illustrative synthetic examples. We then apply the method to the probabilistic absolute hypocenter catalog KaKiOS-16, which contains three decades of South Californian seismicity. To reduce data size and increase computation efficiency, the new approach builds upon the previously introduced catalog condensation method that exploits the heterogeneity of the hypocenter uncertainties. We validate the obtained fault network through a pseudo prospective spatial forecast test and discuss possible improvements for future studies. The performance of the presented methodology attests the importance of the non-linear techniques used to quantify location uncertainty information, which is a crucial input for the large scale application of the method. We envision that the results of this study can be used to construct improved models for the spatio-temporal evolution of seismicity.

1. Introduction

Owing to the continuing advances in instrumentation and improvement of seismic networks coverage, earthquake detection magnitude thresholds have been decreasing while the number of recorded events is increasing. As governed by the Gutenberg-Richter law, the number of earthquakes above a given magnitude increases exponentially as the magnitude is decreased (Ishimoto and Iida, 1939; Gutenberg and Richter, 1954). Recent studies suggest that the Gutenberg-Richter law might hold down to very small magnitudes corresponding to interatomic-scale dislocations (Boettcher et al., 2009; Kwiatek et al., 2010). This implies that there is practically no upper limit on the amount of seismicity we can expect to record as our instrumentation capabilities continue to improve. Although considerable funding and research efforts are being channeled

102 into recording seismicity, when we look at the uses of the end product (i.e. seismic catalogs) we often see that the vast
103 majority of the data (i.e. events with small magnitudes) are not used in the analyses. For instance, probabilistic seismic
104 hazard studies rely on catalogs ~~with large durations~~ containing events detected over long terms, which increases the minimum
105 magnitude that can be considered due to the higher completeness magnitude levels in the past. Similarly, earthquake
106 forecasting models are commonly based on the complete part of the catalogs. For instance, in their forecasting model,
107 (Helmstetter et al., 2007) use only $M > 2$ events, which corresponds to only ~30% of the recorded seismicity. The forecasting
108 skills of the current state-of-the-art models can well be hindered not only due to our limited physical understanding of
109 earthquakes, but also due to this data censoring.

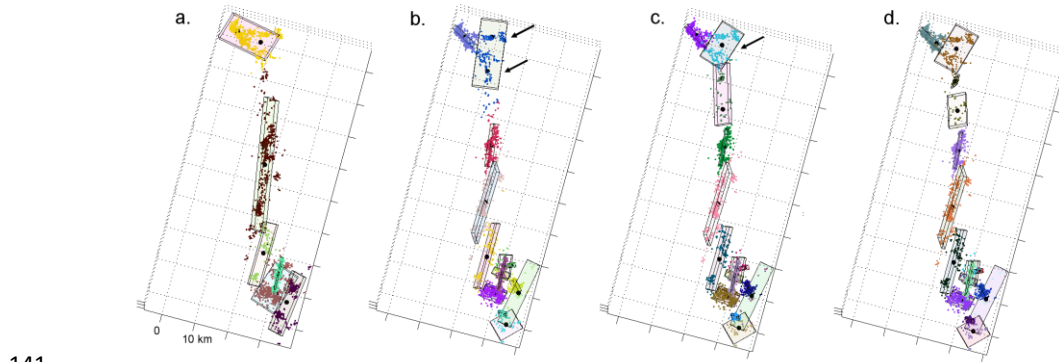
110 In this conjecture, fault network reconstruction can be regarded as an effort to tap into this seemingly neglected but
111 vast data source, and extract information in the form of parametric spatial seismicity patterns. We are motivated by the
112 ubiquitous observations that large earthquakes are followed by aftershocks that sample the main rupturing faults, and
113 conversely that these faults become the focal structures of following large earthquakes. In other words, there is a relentless
114 cycle as earthquakes occur on faults that themselves grow by accumulating earthquakes. By using each earthquake, no
115 matter how big or small, as a spark in the dark, we aim to illuminate and reconstruct the underlying fault network. If the
116 emerging structure is coherent, it should allow us to better forecast the spatial distribution of future seismicity and also to
117 investigate possible interactions between its constituent segments.

118 The paper is structured as follows. First, we give an overview of recent developments in the field of fault network
119 reconstruction and spatial modeling of seismicity. In Section 2, we describe our new clustering method and demonstrate its
120 performance using a synthetic example. In Section 3, we apply the method to the recently relocated southern California
121 catalog KaKiOS-16 (Kamer et al., 2016) and discuss the obtained fault network. In Section 4, we perform a pseudo-
122 prospective forecasting test using four years of seismicity that was recorded during 2011-2015 and was not included in the
123 KaKiOS-16 catalog. In the final Section, we conclude with an outlook on future developments.

124 2. Recent developments in fault reconstruction

125 In the context the work presented here, we use the term "fault" as a three-dimensional geometric shape or kernel
126 optimized to fit observed earthquake hypocenters. Fault network reconstruction based on seismicity catalogs was introduced
127 by (Ouillon et al., 2008). The authors presented a dynamical clustering method based on fitting the hypocenters distribution
128 with a plane, which is then iteratively split into an increasing number of subplanes to provide better fits by accounting of
129 smaller scale structural details. The method uses the overall location uncertainty as a lower bound of the fit residuals to avoid
130 over fitting. (Wang et al., 2013) made further improvements by accounting for the individual location uncertainties of the
131 events and introducing motivated quality evaluation criteria (based, for instance, on the agreement of the planes orientations
132 with the events focal mechanisms). (Ouillon and Sornette, 2011) proposed an alternative method based on probabilistic
133 mixture modeling (Bishop, 2007) using 3D Gaussian kernels. This method introduced notable improvements, such as the use
134 of an independent validation set to constrain the optimal number of kernels to explain the data (i.e. model complexity) and

135 diagnostics based on nearest-neighbors tetrahedra volumes to eliminate singular clusters that cause the mixture likelihood to
136 diverge. While our method is inspired by these studies, and in several aspects builds upon their findings, we also note an
137 inherent drawback of the iterative splitting approach that is common to all the previously mentioned methods. This can be
138 observed when an additional plane (or kernel), introduced by splitting, fails to converge to the local clusters and is instead
139 attracted to the regions of high horizontal variance (see Figure 1 for an illustration in the case of Landers' seismicity).
140



141
142 **Figure 1** Iterative splits on the 1992 Landers aftershock data. Points with different colors represent seismicity associated with each plane.
143 Black dots show the center points of the planes resulting from the next split. Notice how in steps b. to c. step the planes fail to converge to
144 the local branches (shown with arrows), and the method prefers to introduce a horizontal plane to fit a more complex local pattern.

145 This deficiency has motivated us to pursue a different concept. Instead of starting with the simplest model (i.e. a
146 single plane or kernel) and increasing the complexity progressively by iterative splits, we propose just the opposite: start at
147 the highest possible complexity level (as many kernels as possible) and gradually converge to a simpler structure by iterative
148 merging of the individual substructures. In this respect, the new approach can be regarded as a “bottom-up” while the
149 previous ones are “top-down” approaches.

150 3. The agglomerative clustering method

151 3.1. Method description

152 The method shares the basic principles of agglomerative clustering (Rokach and Maimon, 2005) with additional
153 improvements to suit the specifics of seismic data, such as the strong anisotropy of the underlying fault segments. We
154 illustrate the method by applying it to a synthetic dataset obtained by sampling hypocenters on a set of five plane segments,

155 and potentially adding uncorrelated background points which are uniformly distributed in the volume (see Figure 2). The
156 implementation follows the successive steps described below:

157 i) For a given dataset featuring N hypocenters, we first construct an agglomerative hierarchical cluster (AHC) tree
158 based on Ward's minimum variance linkage method (Ward, 1963). Such a tree starts out with a cluster for each data-point
159 (i.e., with zero variance) and then progressively branches into an incrementally decreasing number of clusters (see Figure 2
160 c,d). At any step, the merging of two clusters is based on a criterion involving the minimum distance D_w criterion given by:

$$D_w(C_i, C_j) = \sum_{x \in C_{ij}} (x - r_{ij})^2 - \sum_{x \in C_i} (x - r_i)^2 - \sum_{x \in C_j} (x - r_j)^2 \quad (1)$$

161 In this equation, C_{ij} is the cluster formed by merging clusters C_i and C_j , x represents the set of hypocenters, and r (with
162 proper subscript) is the centroid of each cluster. Hence, clusters i and j are merged if the sum of squares in Eq. (1) is
163 minimized after they are merged into a single cluster ij . The number of branches in the tree is thus reduced by one, and the
164 remaining clusters are used to decide which ones will be merged at the next iteration. This merging of clusters/branches
165 continues until there remains only a single cluster. "Cutting" the AHC tree at the D_w level corresponding to the desired
166 number of branches allows one to choose the number of clusters (from 1 to N) used to represent the original dataset. While
167 there are many different linkage methods and distance metrics, here we have chosen to use Ward's criterion because it
168 produces clusters with regular sizes. This is important for the atomization procedure as we want clusters to have similar
169 potentials to merge and grow into bigger structures.

170 ii) Since our goal is to obtain a fault network where segments are modeled by Gaussian kernels, we begin by
171 estimating how many such kernels can be constructed with the clusters featured in the AHC tree. At its most detailed level
172 (N clusters) no such kernel exists as they would collapse on each data point, becoming singular. At the next level ($N-1$
173 clusters), we have the same problem. We thus incrementally reduce the level, traversing AHC tree, until we get a first cluster
174 featuring 4 hypocenters, which defines the first non-singular cluster. We then continue our traverse along the tree down
175 replacing each cluster having more than 4 points by a Gaussian kernel. At each level on the tree, we count the number of
176 these non-singular Gaussian kernels. The results are illustrated on Figure 2b where we consider two cases: first considering
177 only the 5 planes, the second one including a set of uniformly distributed background points. In the first case, we see that the
178 maximum number of Gaussian kernels (76) is obtained when we cut the tree so that the total number of clusters is 117. In the
179 second case, in the presence of background points, the maximum number of Gaussian kernels (77) is obtained when we cut
180 the tree at a level of 214 clusters. We refer to this maximum number as the "holding capacity" of the dataset, and the
181 corresponding configuration defines the starting point of the following iterative and likelihood-based clustering algorithm.
182 The process of finding this optimum set of initial Gaussian proto-clusters (all containing more than 4 points) is coined as
183 "atomization".

184

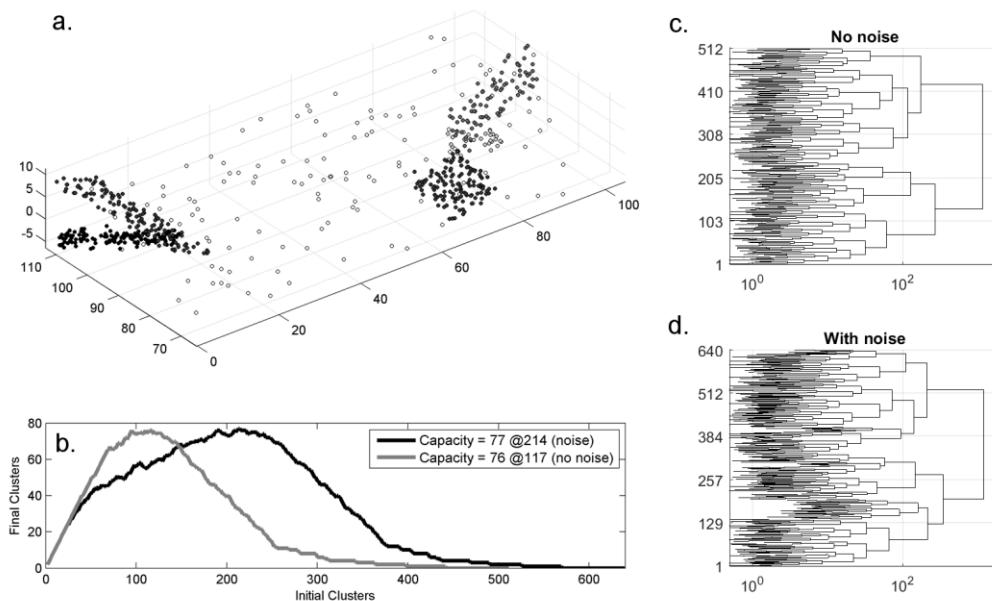


Figure 2 a) Synthetic fault network with 640 points created by uniform sampling of 5 faults, each shown with a different shade according to its total number of points. Empty circles represent the %20 uniformly random background points. b) Determination of the holding capacity (see main text) for the case with and without background points. **c-d) Dendrograms showing the agglomerative hierarchical cluster tree for the data with no noise (c) and with noise (d). The horizontal length of each branch is the minimum distance D_c , (see Eq.1) joining two clusters**

iii) Once we determine the holding capacity, all points that are not associated with any Gaussian kernel are assigned to a uniform background kernel that encloses the whole dataset. The boundaries of this kernel are defined as the minimum bounding box of its points. The uniform spatial density of this background kernel is defined as number of points divided by the volume (see Figure 3). The Gaussian kernels together with the uniform background kernel represent a mixture model where each kernel has a contributing weight proportional to the number of points that are associated with it (Bishop, 2007). This representation facilitates the calculation of an overall likelihood and allows us to compare models with different complexities using the Bayesian Information Criteria (BIC) (Schwarz, 1978) given by:

$$BIC = -\sum_i^N \log(L) + \frac{k}{2} \log(N) \quad (2)$$

Formatted: Font: Italic

Formatted: Font: Italic, Subscript

198 where L is the likelihood of each data point, k is the number of free parameters of the mixture model and N is the total
 199 number of data points. The value of k is calculated as $k=10N_C-1$ (where N_C is the number of kernels in the mixture) since
 200 each kernel requires 3 (mean vector) + 6 (covariance matrix) + 1 (weight) = 10 free parameters. The same parameterization
 201 is also used to describe the background kernel, which is a uniformly dense cuboid with a size and orientation prescribed by
 202 its covariance matrix. The number of free parameters (k) is reduced by 1 because the weights have to sum to unity and hence
 203 knowing N_C-1 of them is sufficient.

204 iv) At the holding capacity, the representation with the large number of kernels ~~are~~-is likely to constitute an
 205 overfitting model for the data set. Therefore, ~~the~~ we iteratively merge pairs of the Gaussian kernels until an optimal balance
 206 between fitness and model complexity is reached. We use the measure of information gain in terms of BIC to select which
 207 pair of kernels to merge. For any given pair of Gaussian kernels, the BIC gain resulting from their merger is calculated using
 208 Equation (3) where L_{int} is the likelihood of each data-point for the initial (unmerged) model and L_{mrg} is the likelihood in the
 209 case where the two candidate clusters are merged:

210

$$\begin{aligned}
 BIC_{Gain} &= BIC_{int} - BIC_{mrg} \\
 BIC_{int} &= -\sum_i^N \log(L_{int}) + \frac{k}{2} \log(N) \\
 BIC_{mrg} &= -\sum_i^N \log(L_{mrg}) + \frac{k-10}{2} \log(N) \\
 BIC_{Gain} &= \sum_i^N \log(L_{mrg}) - \sum_i^N \log(L_{int}) + 5 \log(N)
 \end{aligned} \tag{3}$$

211 Notice that each merging of a pair of kernels decreases k by 10, thus a given merger can be considered only if the reduction
 212 of the penalty term is greater than the decrease of likelihood (i.e. $BIC_{Gain} > 0$).

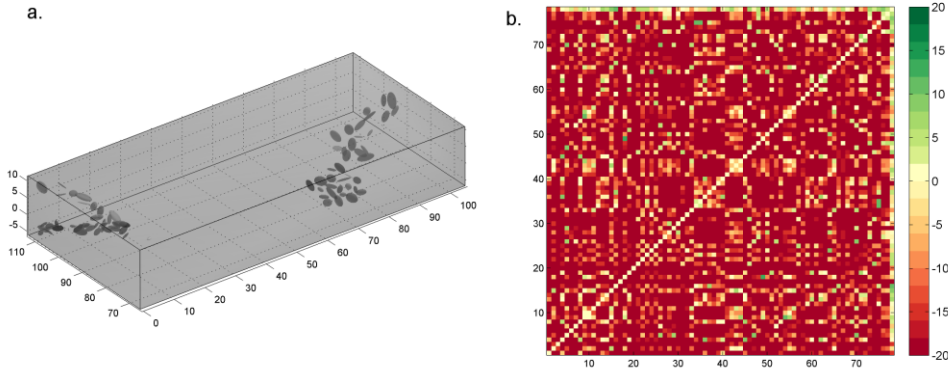


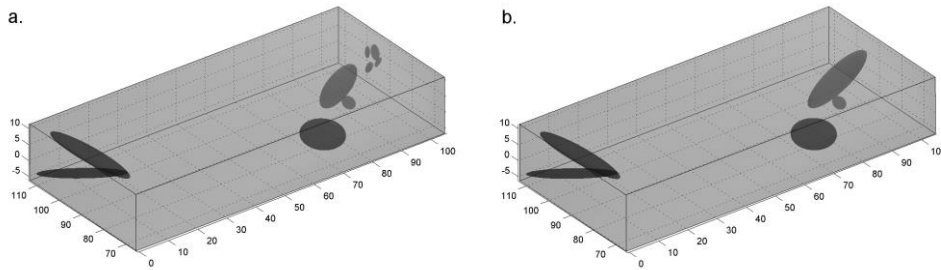
Figure 3 a) The initial *protoclusters* for the synthetic dataset given in [Figure 2a](#). Notice that the number of clusters (78) includes the uniform background kernel as well. b) The *BIC* gain matrix calculated for all possible merging of pairs of kernels.

Using this formulation, we calculate a matrix where the value at the intersection of i^{th} row and j^{th} column corresponds to the BIC gain for merging clusters i and j . We merge the pair with the maximum BIC gain and then re-estimate the matrix since we need to know the BIC gains of the newly formed cluster. At each step, the complexity of the model is reduced by one cluster, and the procedure continues until there is no merging yielding a positive BIC gain. Figure 3b shows such a BIC gain matrix calculated for the initial model with 77 clusters. Notice that a Gaussian cluster is not allowed to merge with the background kernel. The $BIC_{\text{Gain}} > 0$ criteria, which essentially drives and terminates the merging process, is similar to a likelihood ratio test (Neyman and Pearson, 1933; Wilks, 1938) with the advantage that the models tested do not need to be nested.

The computational demand of the BIC gain matrix increases quadratically with the number of data points. To make our approach feasible for large seismic datasets, we introduce a preliminary check that considers clusters as candidates for merging only if they are overlapping within a confidence interval of $\sigma\sqrt{12}$ in any of their principal component directions. The factor $\sqrt{12}$ is derived from the variance of an hypothetical uniform distribution over a planar surface (for details see (Ouillon et al., 2008)).

During all steps of the merging procedure, the data points are in the state of *soft clustering*, meaning that they have a finite probability to belong to any given kernel. A deterministic assignment can be achieved by assigning each point to the kernel that provides the highest responsibility (as per the definition of a mixture model), which is referred to as *hard clustering*. This dichotomy between stochastic and deterministic inference gives rise to two different implementations for the merging criteria: 1) *local* criterion: considering only the two candidate clusters and the data-points assigned to them through hard-clustering and 2) *global* criterion: considering the likelihood of all data-points for all clusters. In essence, the *local* criterion

235 tests the information gain for the case of two kernels versus one kernel on a subset, whereas the global criterion considers N_c
236 versus N_c-1 kernels on the whole mixture and dataset. Figure 4 shows the resulting final reconstructions for the two criteria.
237



238
239 **Figure 4** The final models obtained using the local (a) and global (b) merging criteria for the dataset presented on Figure 2. ~~That~~ the
240 number of clusters, including the uniform background kernel, is 11 and 6 for the local and global criteria respectively.

241 For this synthetic dataset, we observe that both the local and global criteria converge to a similar final structure. The global
242 criterion yields a model with the same number of clusters as the input synthetic, while the local criterion introduces four
243 additional clusters in the under-sampled part of one of the faults. For most pattern recognition applications that deal with a
244 robust definition of noise and signal, the global criterion may be the preferred choice since it is able to recover the true
245 complexity level. However, since this method is indented for natural seismicity, we also see a potential in the local
246 criterion. For instance, consider the case where two fault segments close to each other are weakly active and thus have a low
247 spatial density of hypocenters compared to other distant faults that are much more active. In that case, the global criterion
248 may choose to merge the low-activity faults, while the local criterion may preserve them as separate.

249 3.2. Sensitivity analysis

250 In order to gain insight about the sensitivity and the robustness of the proposed method, we conduct a more elaborate
251 synthetic test. We generate a set of 20 randomly oriented planes with their attributes varying in the following ranges: strike
252 angle -90° to 90° , dip angle 45° to 90° , length 20 to 40 km, width 5 to 15 km. The fault planes span a region with the
253 dimensions of 220 x 150 x 30 km. Each fault plane is sampled randomly with an increasing number of points: starting from
254 0.1 point/km² going up to 2 points/km² in 15 steps, producing sets with a total number of points in the range of 609 to
255 14.475. We also consider three different uniform background noise levels at 5%, 10% and 20% yielding a total of 45
256 synthetic sets. We apply our clustering method to each of these sets and report the resulting performance using the Rand
257 index. The Rand index measures the similarity between different clusterings and is expressed by the following equation

Formatted: Indent: First line: 1.02 cm

Formatted: Superscript

$$R = \frac{2(a+b)}{n(n-1)} \quad (4)$$

where a is the number of pairs that are in the same cluster in the two clusterings, b is the number of pairs that are in different clusters in the two clusterings and n is the number of points in the dataset. A Rand index of 1 indicates total match between the two groupings while a value of 0 indicates that all pairs are in disagreement. In our case, we are comparing the ground truth clustering, which is given by the 20 fault planes and the uniform background, and the clustering obtained by our method. Figure 5a shows the Rand index obtained using the *local* and the *global* criteria as a function of increasing sampling density for the three levels of background noise. As mentioned earlier, the performance of the *global* criterion is better than the *local* one, which degrades with increasing density as the method start introducing additional clusters. The Rand index of the *global* criterion saturates around 0.95 and starts decreasing as the density increases above ~ 1.25 points/km². This saturation can be explained by the fact that additional Gaussian kernels are needed to fit the sharp corners of the rectangular planes as they become more pronounced with increased sampling. We can make an analogy with the Fourier series expansion of a square wave, where more terms are needed to fit the sharp edges. In our case, these additional terms (i.e. Gaussian kernels) increase the complexity and cause the Rand index to drop. To confirm this we repeat the synthetics by sampling Gaussian kernels with the eigenvectors corresponding to the rake and dip, and eigenvalues corresponding to the length, width and thickness of the rectangular planes. The results are shown in Figure 5b where we see no drop off in the Rand index.

Formatted: Indent: First line: 1.02 cm

Formatted: Font: Italic

Formatted: Font: Italic

Formatted: Font: Italic

Formatted: Font: Italic

Formatted: Font: Italic

Formatted: Font: Italic

Formatted: Font: Italic

Formatted: Superscript

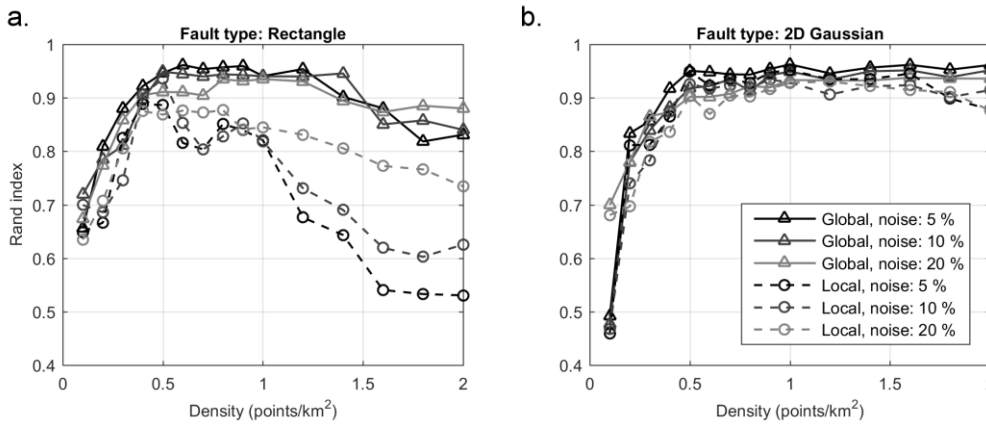


Figure 5 Clustering similarities between ground truth synthetic dataset and method results quantified by the Rand index. *Global* and *Local* merging criteria are shown as solid and dashed lines respectively. Background noise amplitude is shown as shades of gray. Results for ground truth sampled from a) rectangular fault planes b) elliptic Gaussian kernels with similar dimensions.

Formatted: Font: Italic

Formatted: Font: Italic

279 These synthetics indicate that the method is robust in the presence of uniform background noise and that it is able to
280 recover structures that are sufficiently sampled. In the presented case, the performance saturates around 0.5 points/km²,
281 however this value can change based on the particular setting. For instance, if faults are very closely spaced and intersecting,
282 higher sampling may be needed. On the other hand, if the structures are isolated, similar performance can be achieved at
283 lower sampling. The MATLAB code used for generating the synthetics and evaluating the reconstruction's Rand index is
284 provided. Users may prefer to create synthetic cases that are informed by the properties of the actual data they are working
285 on (such as numbers of points, spatial extend, etc.)

286 4. Application to seismicity

287 In this section, we apply our method to observed seismicity data. For this purpose, we use the KaKIOS-16 catalog
288 (Kamer et al., 2016) that was obtained by probabilistic absolute location of nearly 479,000 Southern Californian events
289 spanning the time period 1981-2011. We consider all events, regardless of magnitude, as each event samples some part of
290 the fault network. Before tackling this vast dataset, however, we first consider the 1992 Landers sequence as a smaller
291 dataset to assess the overall performance and computational demands.

292 4.1. Small Scale application to the Landers aftershocks sequence

293 We use the same dataset as (Wang et al., 2013) that consists of 3,360 aftershocks of the 1992 Landers earthquake.
294 The initial atomization step produces a total of 394 proto-clusters that are iteratively merged using the two different criteria
295 (local and global). The resulting fault networks are given in Figure 6 together with the fault traces available in the
296 Community Fault Model of southern California (Plesch et al., 2007). Comparing the two fault networks, we observe that the
297 local criterion provides a much detailed structure that is consistent with the large scale features in the global one. We also
298 observe that, in the southern end, the global criterion produces thick clusters by lumping together small features with
299 seemingly different orientations. These small scale features have relatively few points and thus low contribution to the
300 overall likelihood. The global criterion favors these mergers to reduce the complexity penalty in Equation (2), which scales
301 with the total number of points. In the local case, however, because each merger is evaluated considering only the points
302 assigned to the merging clusters, the likelihood gain of these small scale features can overcome the penalty reduction and
303 they remain unmerged. It is also possible to employ metrics based on consistency of focal mechanism solutions to evaluate
304 the reconstructed faults. For a detailed application of such metrics the reader is referred to the detailed work by Wang et
305 al.(2013). In this study, since we do not have focal mechanism solutions for our target catalog, we focus on information
306 criteria metrics and out of sample forecast tests.
307

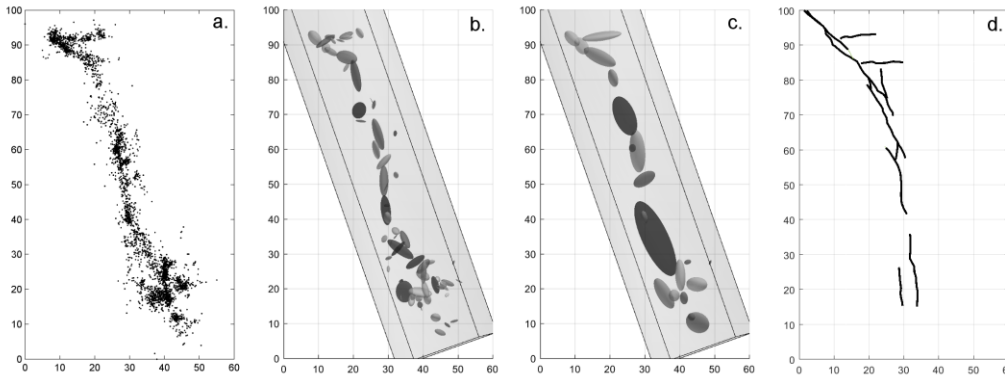


Figure 6 a) Top view of the 1992 Landers aftershocks. Fault networks obtained from these events using the local (b) and global (c) merging criterion, each resulting in 70 and 22 clusters respectively. d) Fault traces obtained from the [Community Fault Model of southern California](#)

Our second observation is that the background kernel attains a higher weight of 11% using the local criterion compared to the global one yielding only 5%. Keeping in mind that both criteria are applied on the same initial set of proto-clusters, and that there are no mergers with the background kernel, we argue that the difference between the background weights is due to density differences in the tails of the kernels. We investigate this in Figure 7 for the simple 1D case considering mergers between two boxcar functions (analogous for planes in 3D) approximated with Gaussian functions. We observe that the merged Gaussian has higher densities in its tails compared to its constituents. The effect is amplified when the distance between the merging clusters is increased (Figure 7b). Hence, in the local case, the peripheral points are more likely to be associated with the background kernel due to the lower densities at the tails of the small, unmerged clusters.

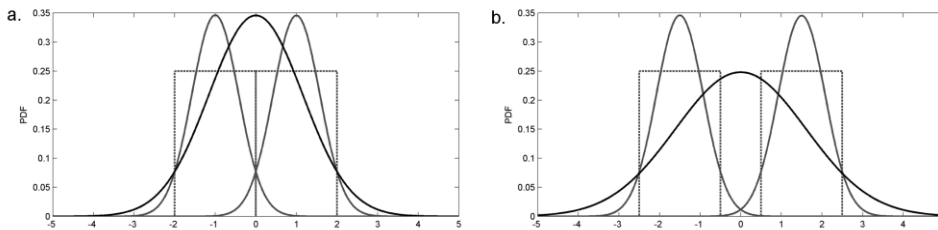


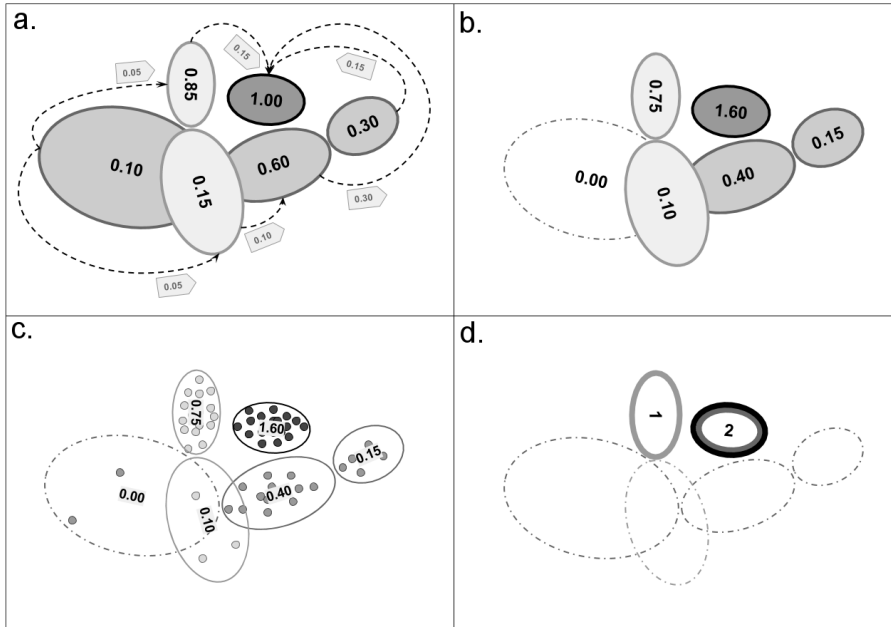
Figure 7 Two uniform distributions (dotted gray lines), their Gaussian approximations (solid gray lines) and the Gaussian resulting from their merger (solid black line). Notice that the joint Gaussian has higher densities at the tails compared to its constituents.

324 Another important insight from this sample case was regarding the feasibility of a large scale application. As
325 pointed out here and in previous studies (Ouillon and Sornette, 2011; Wang et al., 2013), the computational demand for such
326 pattern recognition methods increases rapidly with the number of data-points. The Landers case with 3,360 points took ~5
327 minutes on a 4-core, 2.2GHz machine with 16GB memory. Considering that our target catalog is nearly ~145 times larger, a
328 quadratic increase would mean an expected computation time of more than two months. Even with a high performance
329 computing cluster, we would have to tackle memory management and associated overhead issues. Although technically
330 feasible, pursuing this path would limit the use of our method only to the few privileged with access to such computing
331 facilities. In a previous work we proposed a new solution called "catalog condensation", that uses the location uncertainty
332 estimates to reduce the length of a catalog while preserving its spatial information content (Kamer et al., 2015). In the
333 following section, we will detail how we applied this method to the KaKiOS-16 catalog in order to make the clustering
334 computations feasible.

335 4.2. Condensation of the KaKiOS-16 catalog

336 The condensation method reduces the effective catalog length by first ranking the events according to their location
337 uncertainty and then successively condensing poorly located events onto better located ones (for detailed explanation see
338 Kamer et al., 2015). The initial formulation of the method was developed considering the state of the art catalogs of the time.
339 Location uncertainties in these catalogs are assumed to be normally distributed and hence expressed either in terms of a
340 horizontal and vertical standard deviation, or with a diagonal 3×3 covariance matrix. With the development of the KaKiOS-
341 16 catalog, we extended this simplistic representation to allow arbitrarily complex location PDFs to be modeled with
342 mixtures of Gaussians. Such mixture models, consisting of multiple Gaussian kernels, ~~was~~were found to be the optimal
343 representation for 81% percent of the events, which required an average of 3.24 Gaussian components (the rest was
344 optimally modeled using a single Gaussian kernel). Therefore we first needed to generalize the condensation methodology,
345 which was initially developed for single kernels, to accommodate the multiple kernel representation. In the original version,
346 all events are initiated with equal unit weights. They are then ranked according to their isotropic variances and weights are
347 progressively transferred from the high variance to the low variance events according to their overlap. In the generalized
348 version, each event is represented by a number of Gaussian kernels that are initiated with their respective mixture weight (0-
349 1). All kernels are then ranked according to their isotropic variance and the weights are transferred as in the original method
350 with the additional constraint that weight transfers between kernels of the same event are not allowed (see Figure 8a, b). This
351 constraint is motivated by the fact that the kernels representing each event's location PDF are already optimized. Thus a
352 weight transfer between those can lead only to a sub-optimal location representation.

353



354
355
356
357
358
359

Figure 8 Idealized schematic representations of 3 events with 1,2 and 3 Gaussian kernels each a) Condensation: each event is represented by a different shade, weight transfer is represented by the arrows; notice that there are no intra-event weight transfers b) Final condensed catalog: the total weight sum is preserved, one component is discarded. c) Sampling of the event PDFs: this step is done on the original catalog d) Each event is assigned to the condensed kernel that provides the maximum likelihood for most of its sampled points; three events are assigned to two condensed kernels.

360
361
362
363
364
365
366
367
368

The KaKiOS-16 catalog contains 479,056 events whose location PDFs are represented by a total of 1,346,010 Gaussian components (i.e. kernels). Condensation reduces this number to 600,463 as weights from events with of-high variance are transferred to better located ones. Nevertheless, in Figure 9 we see that nearly half of these components amount to only 10% of the total event weight. The computation time scales with the number of components, while the information content is proportional to number of events. Hence the large number of components amounting to a relatively low number of events would make the computation inefficient. A quick solution could be to take the components with the largest weights constituting 90% or 95% of the total mass, mimicking a confidence interval. Such a "solution" would depend on the arbitrary cutoff choice and would have the potential to discard data that may be of value for our application.

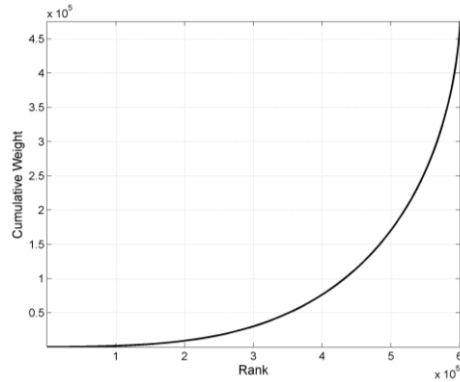


Figure 9 Cumulative weights of the 600,463 condensed KaKiOS-16 components representing a total of 479,056 events. The components are ranked according to increasing weights.

We can avoid such an arbitrary cut-off by employing the fact that the condensed catalog is essentially a Gaussian mixture model (GMM) representing the spatial PDF of earthquake occurrence in South California. We can then, in the same vein as the hard clustering described previously, assign each event to its most likely GMM component (i.e. kernel). If we consider each event individually, the most likely kernel would be the one with the highest responsibility. However, for a globally optimal representation we need to find the best representative kernel for each event among all other kernels. To do this, we sample the original (uncondensed) PDF of each event with 1000 points and then calculate the likelihood of each sample point with respect to all the condensed kernels. The event is assigned to the kernel that provides the maximum likelihood for the highest number of sample points (see Figure 8c,d). As a result of this procedure, the 479,056 events are assigned to 93,149 distinct kernels. The spatial distribution of all the initial condensed kernels is given in Figure 10a, while the kernels assigned with at least one event after the hard clustering are shown in Figure 10b. Essentially, this procedure can be viewed as using the condensed catalog as a prior for the individual event locations. The use of accumulated seismicity as a prior for focusing and relocation has been proposed by Jones and Stewart (1997) and investigated in detail by Li et al. (2016). We can see the effect of this strategy more clearly in Figure 8, where starting from 3 different events in the catalog (Figure 8a), we finally converge to only 2 different final locations (Figure 8d).

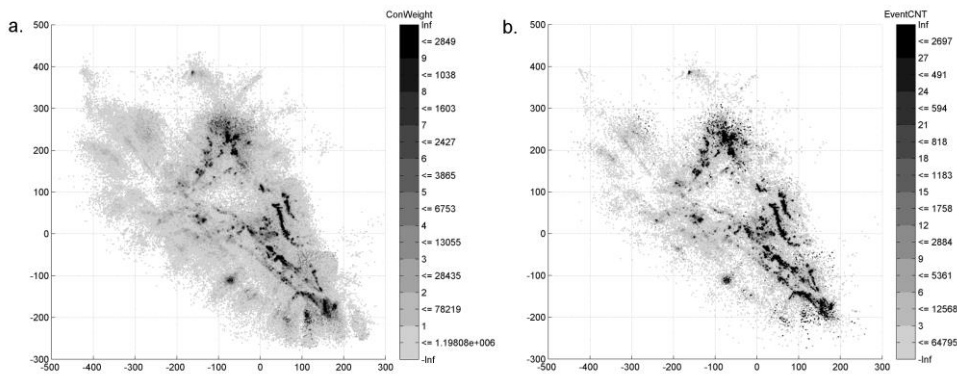


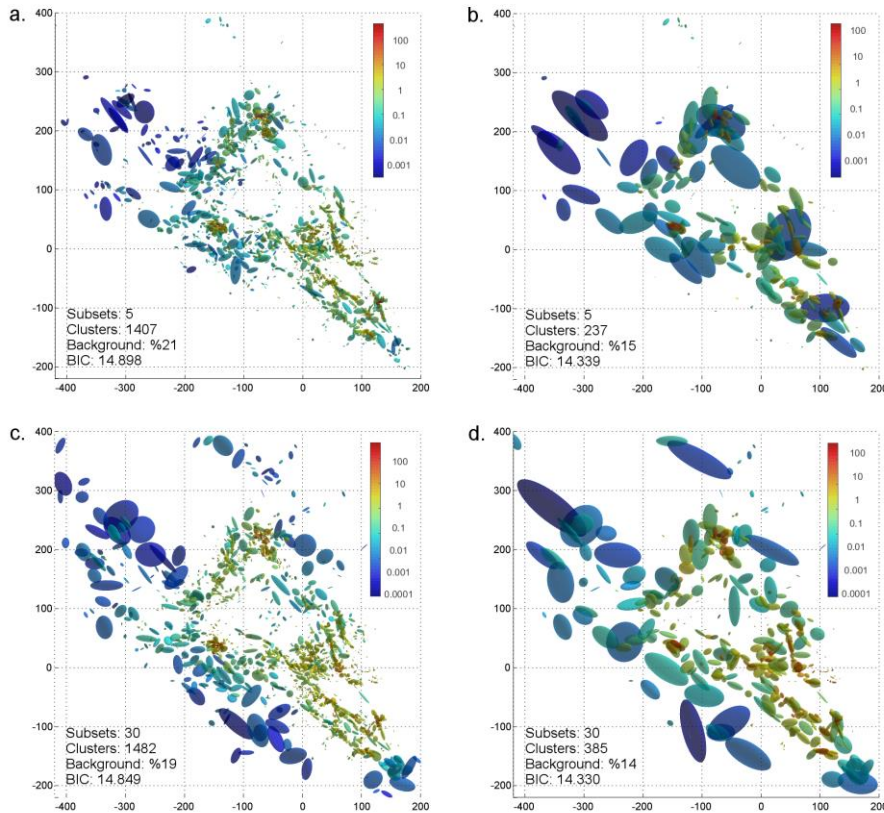
Figure 10 a: Mean locations of condensed 600,463 Gaussian components shaded according to their weights. b: The same components shaded according to the total number of events assigned to them after the maximum likelihood assignment

4.3. Large scale application to Southern California

In previous works, we concluded that the spatial distribution of southern California seismicity is multifractal, i.e. it is an inhomogeneous collection of singularities (Kamer et al., 2015, 2016). The spatial features in Figure 10 can be seen as expressions of these singularities. Since we are interested in the general form of the fault network rather than the second order features (e.g. inhomogeneous seismicity rates along the same fault) we consider all the centers of all 93,149 kernels as individual points, effectively disregarding their weights. Considering the weight of each kernel would result in more complex structure with singularities that can be associated with the fractal slip distribution of large events (Mai and Beroza, 2002) modulated through the non-uniform network detection capabilities. Thus, by disregarding the kernel weights we are considering only the potential loci of earthquakes, not their activity rates.

Another important aspect, in the case of such a large scale application, is the uniform background kernel. The assumption of a single background kernel defined as the minimum bounding box of the entire dataset seems to be suitable for the case of Landers aftershocks, however it becomes evident that for whole Southern California such a minimum bounding box would overestimate the data extent (covering aseismic offshore areas) and would thus lead to an underestimated density. In addition, one can also expect the background density to vary regionally in such large domains. We thus extend our approach by allowing for multiple uniform background kernels. For this purpose, we make use of the AHC tree that is already calculated for the atomization of the whole dataset. We then cut the tree at a level corresponding to only a few clusters (5 or 30 in the following application), which allows to divide the original catalog into the smaller subcatalogs represented by each cluster. Each of these subsets is then atomized individually yielding its own background kernel. The atomized subsets are then brought together, to be progressively merged. Naturally, we have no objective way of knowing how many background kernels a dataset may feature. However, in various synthetic tests, involving cuboid

409 backgrounds with known densities, we observe that inflating this number has no effect on the recovered densities, whereas a
410 too low value causes underestimation. Apart from this justification, we are motivated to divide this large dataset into subsets
411 for purely computational reasons as this allows for improved parallelization and computational efficiency.



412
413 **Figure 11** Fault network reconstructions for the KaKiOS-16 catalog. Top row shows results for the case of 5 initial subsets with (a) local
414 and (b) global merging criterion. Bottom row shows the (c) local and (d) global -merging criterion for 30 initial subsets. The number of
415 clusters, background weight and BIC per data point is given in the insets. Clusters are colored according their density (data point per km³)
416 where the volume is estimated as the product of standard deviations along the principal component axes.

Formatted: Superscript

417 Figure 11 shows the two fault networks obtained for two different initial settings: using 5 and 30 subsets. For each
418 choice, we show the results of the local and global criterion; the background cuboids are not plotted to avoid clutter. Our

419 immediate observation is related to the events associated with the 1986 Oceanside sequence (Wesson and Nicholson, 1988)
420 located at coordinates (-75,-125). The kernel associated with these events is virtually absent in the fault networks
421 reconstructed from 5 initial subsets (Figure 11a,b). This can be explained in terms of the atomization procedure. In the case
422 of 5 initial subsets, the offshore Oceanside seismicity falls in a subset containing onshore faults such as the Elsinore fault at
423 coordinates (0,-75). Because these faults have a more coherent spatial structure compared to the diffused Oceanside
424 seismicity, their proto-cluster holding capacity is higher. Hence the atomization procedure continues increasing the number
425 of clusters while the Oceanside seismicity has actually reached its own holding capacity. This causes nearly all of the proto-
426 clusters within the Oceanside region to become singular and be discarded into the background. In the case of 30 subsets, the
427 Oceanside seismicity is in a separate region and thus is able to retain a more reliable holding capacity estimation, yielding to
428 the detection of the underlying structures.

429 At this point, the natural question would be: which of these fault networks is a better model? The answer to this
430 question would depend on the application. If one is interested in the correspondence between the reconstructed faults and
431 focal mechanisms, or high resolution fault traces, which are expressions of local stress/strain conditions, then the ideal
432 choice would be the local criterion. However, if the application of interest is an earthquake forecast covering the whole
433 catalog domain, then one should consider the global criterion because it yields a lower BIC value, since it is formulated with
434 respect to the overall likelihood. We leave the statistical investigation of the fault network parameters (e.g. fault length, dip,
435 thickness distributions) as a subject for a separate study and instead focus on an immediate application of the obtained fault
436 networks.

437 5. Validation through a spatial forecast test

438 Several methods can be proposed for the validation of a reconstructed fault network. One way could be to project
439 the faults on the surface and check their correspondence with the mapped fault traces. This would be a tedious task since it
440 would involve a case-by-case qualitative analysis. Furthermore, many of the faults illuminated by recent seismicity might not
441 have been mapped or they may simply have no surface expressions. In the case of the 2014 Napa earthquake, there was also
442 a significant disparity between the spatial distribution of aftershocks and the observed surface trace (Brocher et al., 2015).
443 Another option would be to compare the agreement between the reconstructed faults and the focal mechanisms of the events
444 associated with them. With many of the metrics already developed (Wang et al., 2013), this would allow for a systematic
445 evaluation. However, the current focal mechanisms catalog for Southern California is based on the HYS-12 catalog
446 (Hauksson et al., 2012; Yang et al., 2012) obtained by relative double-difference techniques. As previously discussed in our
447 studies (Kamer et al., 2015, 2016), we have demonstrated that this catalog exhibits artificial clustering effects at different
448 scales. Hence, any focal mechanism based on hypocenters from this relative location catalog would be inconsistent with the
449 absolute locations of the KaKiOS-16 catalog.

450 Therefore we are left with the eventual option: validation by spatial forecasting. For this purpose, we will use the
451 global criterion model obtained from 30 subsets because it has the lowest BIC value of the four reconstructions presented

452 above. Our fault reconstruction uses all events in the KaKiOS-16 catalog, regardless of their magnitude. The last event in
453 this catalog occurred on June 30th 2011. For target events, we consider all routinely located events by the Southern California
454 Earthquake Data Center between July 1st 2011 and July 1st 2015 with magnitudes larger than M2.5. We limit our volume of
455 interest arbitrarily to the region limited by latitudes [32.5, 36.0], longitudes [-121, -115] and depths in the range 0-20km. The
456 likelihood scores of the target events are calculated directly from the fault network, which is essentially a weighted mixture
457 of Gaussian PDFs and uniform background kernels. The only modification done to accommodate the forecast is aggregating
458 all background kernels into a single cuboid covering the volume of interest. The weight of this cuboid is equal to the sum of
459 all aggregated background kernel weights. To compare the spatial forecasting performance of our fault network we consider
460 the simple smoothed seismicity model (TripleS) (Zechar and Jordan, 2010) that was proposed as a forecasting benchmark.
461 This model is obtained by replacing each event with an isotropic, constant bandwidth Gaussian kernel. The bandwidth is
462 then optimized by dividing the dataset into training and validation sets. As already pointed out by (Zechar and Jordan, 2010)
463 the construction of the model involves several choices (e.g. choice of optimization function, choice of candidate bandwidths,
464 etc...). To sidestep these choices we construct the TripleS model by optimizing the bandwidth parameter directly on the
465 target set. Allowing this privilege of foresight, which would not be possible in a prospective setting, makes sure that the
466 TripleS method is at its maximum attainable forecast skill. Figure 12 shows the forecast performances of our fault network,
467 the TripleS model and a single uniformly dense cuboid. The performance is quantified in terms of negative log likelihood per
468 target event for varying magnitude cut-offs of the target dataset. The reconstructed fault network performs better for all
469 magnitude cut-off levels. We also observe a consistent relative performance increase with increasing magnitude cutoff,
470 suggesting that the larger events tend to occur closer to the principal planes defined by the two largest eigenvalues of the
471 fitting kernels.

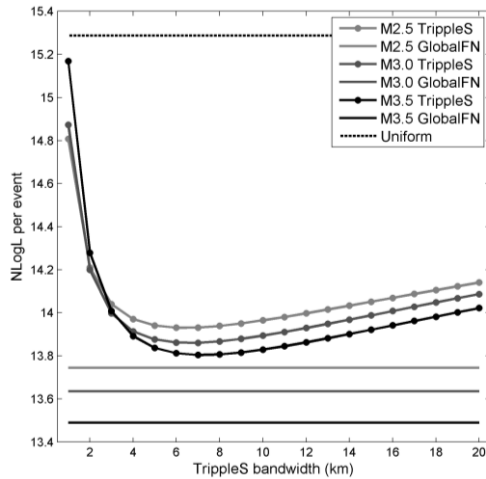


Figure 12 Average Negative Log Likelihood for the target dataset limited to events above M2.5 (light gray), M3.0 (dark gray) and M3.5 (black). Performance of the TripleS models is evaluated as a function of the isotropic kernel bandwidth (dotted lines). The fault network performance is plotted with constant level solid lines. The performance of a single uniformly dense cuboid is plotted with a dashed line.

The superiority of our model with respect to TripleS can be understood in terms of model parameterization, i.e. model complexity. There is a general misconception regarding the meaning of “[model complexity](#)” [in the earthquake forecasting community as it relates to a statistical](#). The term is often used to express the degree of conceptual convolution employed while deriving the model. For instance, in their 2010 paper, Zechar and Jordan refer to the TripleS model as “a simple model” compared to models employing anisotropic or adaptive kernels (Kagan and Jackson, 1994, 2007). As a result, one might be inclined to believe that the model obtained by fault reconstruction presented in this study is far more complex than TripleS. However, it is important to notice that the complexity of a model is independent of the algorithmic procedures undertaken to obtain it. What matters is the number of parameters that are needed to communicate it, or in other words its minimum description length (Rissanen, 1978; Schwarz, 1978). TripleS is essentially a GMM model expressed by the 3D locations of its components and a constant kernel bandwidth. Hence it has a total of $(3 \times 479,056) + 1 = 1,437,168$ free parameters compared to the $(10 \times 385) - 1 = 3,849$ of our fault network. Thus, the difference in spatial forecasting performance can be understood in terms of the TripleS’ overparameterization compared to the optimal complexity criteria employed in reconstructing the fault network. It is true that, compared to our fault reconstruction method, the TripleS model is easier to formulate and obtain. However, the fact that the isotropic TripleS kernels are co-located with hypocenters of previous earthquakes does not reduce the complexity of the model. As an everyday analogy, consider for instance an image saved as Bitmap, where each pixel is encoded with an integer representing its color: Such a representation of an image, although much simpler to encode, would require larger storage space compared to one obtained by JPEG compression. Although the

493 | JPEG compression is an elaborated algorithm, it produces a representation that is much simpler. In the same vein, the fault
494 reconstruction method uses regularities in the data to obtain a simpler, more optimal representation.

495 | Another contributing factor to the performance of the fault network can be regarded as the utilization of location
496 uncertainty information that facilitates condensation. This has two consequences: 1) decreasing the overall spatial entropy
497 and thus providing a clearer picture of the fault network, and 2) reducing the effect of repeated events occurring on each
498 segment, thus providing a more even prior on all segments.

499 | 6. Conclusion

500 | We presented an agglomerative clustering method for seismicity-based fault network reconstruction. The method
501 provides the following advantages: 1) a bottom-up approach that explores all possible merger options at each step and moves
502 coherently towards a global optimum; 2) an optimized atomization scheme to isolate the background (i.e. uncorrelated)
503 points; 3) improved computation performance due to geometrical merging constraints. We were able to analyze a very large
504 dataset consisting of 30 years of South Californian seismicity by utilizing the non-linear location uncertainties of the events
505 and condensing the catalog to ~20% of its initial size. We validated the information gain of the reconstructed fault network
506 through a pseudo-prospective 3D spatial forecast test, targeting 4 years of seismicity.

507 | Notwithstanding these encouraging results, there are several aspects in which the proposed methodology can be
508 further improved and extended. In the current formulation, the distinct background kernels are represented by the minimum
509 bounding box of each subset, so that they tend to overlap and bias the overall background density. This can be improved by
510 employing convex hulls, alpha shapes (Edelsbrunner and Mücke, 1994) or a Voronoi tessellation (Voronoi, 1908) optimized
511 to match the subset borders. The shape of the background kernel could also be adapted to the specific application; for
512 induced seismicity catalogs, it can be a minimum bounding sphere or an isotropic Gaussian since the pressure field diffuses
513 more or less radially from the injection point (Király-Proag et al., 2016). Different types of proto-clusters such as Student-t
514 kernels or copulas can be used in the atomization step or they can be introduced at various steps of the merger by allowing
515 for data-driven kernel choices.

516 | The reconstructed faults can facilitate other fault related research by providing a systematic way to obtain planar
517 structures from observed seismicity. For instance, analysis of static stress transfer can be aided by employing the
518 reconstructed fault network to resolve the focal plane ambiguity (Nandan et al., 2016; Navas-Portella et al., 2020). Similarly,
519 the orientation of each individual kernel can be used as a local prior to improve the performance of real-time rupture
520 detectors (Böse et al., 2017). Studies relying on mapped fault traces to model rupture dynamics can be also extended using
521 reconstructed fault networks that represent observed seismicity including its uncertainty (Wollherr et al., 2019).

522 | An important implication of the reconstructed fault network is its potential in modeling the temporal evolution of
523 seismicity. The Epidemic Type Aftershock Sequence (ETAS) model can be simplified significantly in the presence of
524 optimally defined Gaussian fault kernels. Rather than expressing the whole catalog sequence as the weighted combination of
525 all previous events, we can instead coarse-grain the problem at the fault segment scale, and have multiple sequences

526 corresponding to each fault kernel, each of them being a combination of the activity on the other fault kernels. Such a
527 formulation would eliminate the need for the commonly used isotropic distance in the ETAS kernels, as this single degree
528 kernel induces essentially the same deficiencies discussed in the case of the TripleS model. Thus, we can expect such an
529 ETAS model, based on a fault network, to have significantly better forecasting performances compared to its isotropic
530 variants.

531

532 **Code and data availability.** The Matlab implementation of the agglomerative fault reconstruction method and the synthetic
533 tests can be downloaded from <http://www.mathworks.com/matlabcentral/fileexchange/81193> (last accessed October 2020).
534 The KaKiOS-16 catalog can be downloaded from <http://www.ykamer.xyz/kakios/> (last accessed July 2020). The Matlab
535 implementation of the condensation method can be downloaded from
536 <http://www.mathworks.com/matlabcentral/fileexchange/48702> (last accessed July 2020).

537

538 **Author contributions.** All authors conceived and designed the research. YK wrote the paper with major contributions GO
539 and DS. YK developed the computer codes.

540

541 **Competing interests.** The authors declare that they have no conflict of interest.

542

Formatted: Indent: First line: 0 cm

543 Acknowledgments

544 We would like to thank our two reviewers Leandro C. Gallo and Nadav Wetzler for their valuable comments and
545 suggestions, which improved this paper considerably.

546

547 References

- 548 Bishop, C. M. (2007), *Pattern Recognition and Machine Learning*, Springer.
- 549 Boettcher, M. S., A. McGarr, and M. Johnston (2009), Extension of Gutenberg-Richter distribution to $M_W -1.3$, no lower
550 limit in sight, *Geophys. Res. Lett.*, 36(10), L10307, doi:10.1029/2009GL038080.
- 551 Böse, M., D. E. Smith, C. Felizardo, M.-A. Meier, T. H. Heaton, and J. F. Clinton (2017), FinDer v.2: Improved real-time
552 ground-motion predictions for M2–M9 with seismic finite-source characterization, *Geophys. J. Int.*, 212(1), 725–742,
553 doi:10.1093/gji/ggx430.
- 554 Brocher, T. M., A. S. Baltay, J. L. Hardebeck, F. F. Pollitz, J. R. Murray, A. L. Llenos, D. P. Schwartz, J. L. Blair, D. J.

555 Ponti, J. J. Lienkaemper, et al. (2015), The Mw 6.0 24 August 2014 South Napa Earthquake, *Seismol. Res. Lett.*,
556 86(2A), 309–326, doi:10.1785/0220150004.

557 Edelsbrunner, H., and E. Mücke (1994), Three-dimensional alpha shapes, *ACM Trans. Graph.*, 13(1), 43–72.

558 Gutenberg, B., and C. F. Richter (1954), *Seismicity of the earth and associated phenomena*, [2d. ed.], Princeton University
559 Press, Princeton N.J.

560 Hauksson, E., W. Yang, and P. M. Shearer (2012), Waveform relocated earthquake catalog for Southern California (1981 to
561 June 2011), *Bull. Seismol. Soc. Am.*, 102(5), 2239–2244.

562 Helmstetter, A., Y. Y. Kagan, and D. D. Jackson (2007), High-resolution Time-independent Grid-based Forecast for M5
563 Earthquakes in California, *Seismol. Res. Lett.*, 78(1), 78–86, doi:10.1785/gssrl.78.1.78.

564 Ishimoto, M., and K. Iida (1939), Observations sur les seismes enregistres par le microsismographe construit dernièrement,
565 *Bull. Earthq. Res. Inst. Univ. Tokyo*, 17, 443–478.

566 Jones, R. H., and R. C. Stewart (1997), A method for determining significant structures in a cloud of earthquakes
567 Simplifying the Earthquake Cloud, *J. Geophys. Res.*, 102(134), 8245–8254.

568 Kagan, Y. Y., and D. D. Jackson (1994), Long-term probabilistic forecasting of earthquakes, *J. Geophys. Res.*, 99(B7),
569 13685–13700, doi:10.1029/94JB00500.

570 Kagan, Y. Y., and D. D. Jackson (2007), Forecast for $M \geq 5$ Earthquakes in California, , 78(1).

571 Kamer, Y., G. Ouillon, D. Sornette, and J. Wössner (2015), Condensation of earthquake location distributions: Optimal
572 spatial information encoding and application to multifractal analysis of south Californian seismicity, *Phys. Rev. E*,
573 92(2), 022808, doi:10.1103/PhysRevE.92.022808.

574 Kamer, Y., E. Kissling, G. Ouillon, and D. Sornette (2016), KaKiOS-16: a probabilistic, non-linear, absolute location catalog
575 of the 1981-2011 Southern California seismicity, *Bull. Seismol. Soc. Am.*

576 Király-Proag, E., J. D. Zechar, V. Gischig, S. Wiemer, D. Karvounis, and J. Doetsch (2016), Validating induced seismicity
577 forecast models-Induced Seismicity Test Bench, *J. Geophys. Res. Solid Earth*, 121(8), 6009–6029,
578 doi:10.1002/2016JB013236.

579 Kwiatek, G., K. Plenkers, M. Nakatani, Y. Yabe, G. Dresen, and JAGUARS-Group (2010), Frequency-magnitude
580 characteristics down to magnitude -4.4 for induced seismicity recorded at Mponeng Gold Mine, South Africa, *Bull.*
581 *Seismol. Soc. Am.*, 100(3), 1165–1173, doi:10.1785/0120090277.

- 582 Li, K. L., Ó. Gudmundsson, A. Tryggvason, R. Bödvarsson, and B. Brandsdóttir (2016), Focusing patterns of seismicity with
583 relocation and collapsing, *J. Seismol.*, 20(3), 771–786, doi:10.1007/s10950-016-9556-x.
- 584 Mai, P. M., and G. C. Beroza (2002), A spatial random field model to characterize complexity in earthquake slip, *J.*
585 *Geophys. Res. Solid Earth*, 107(B11), ESE 10-1-ESE 10-21, doi:10.1029/2001JB000588.
- 586 Nandan, S., G. Ouillon, J. Woessner, D. Sornette, and S. Wiemer (2016), Systematic assessment of the static stress triggering
587 hypothesis using interearthquake time statistics, *J. Geophys. Res. Solid Earth*, 121(3), 1890–1909,
588 doi:10.1002/2015JB012212.
- 589 Navas-Portella, V., A. Jiménez, and Á. Corral (2020), No Significant Effect of Coulomb Stress on the Gutenberg-Richter
590 Law after the Landers Earthquake, *Sci. Rep.*, 10(1), 1–13, doi:10.1038/s41598-020-59416-2.
- 591 Neyman, J., and E. Pearson (1933), On the Problem of the Most Efficient Tests of Statistical Hypotheses, *Philos. Trans. R.*
592 *Soc. London*, 231, 289–337.
- 593 Ouillon, G., and D. Sornette (2011), Segmentation of fault networks determined from spatial clustering of earthquakes, *J.*
594 *Geophys. Res.*, 116(B2), 1–30, doi:10.1029/2010JB007752.
- 595 Ouillon, G., C. Ducorbier, and D. Sornette (2008), Automatic reconstruction of fault networks from seismicity catalogs:
596 Three-dimensional optimal anisotropic dynamic clustering, *J. Geophys. Res.*, 113(B1), 1–15,
597 doi:10.1029/2007JB005032.
- 598 Plesch, A., J. H. Shaw, C. Benson, W. A. Bryant, S. Carena, M. Cooke, J. Dolan, G. Fuis, E. Gath, L. Grant, et al. (2007),
599 Community Fault Model (CFM) for Southern California, *Bull. Seismol. Soc. Am.*, 97(6), 1793–1802,
600 doi:10.1785/0120050211.
- 601 Rissanen, J. (1978), Modeling by shortest data description, *Automatica*, 14(5), 465–471, doi:10.1016/0005-1098(78)90005-
602 5.
- 603 Rokach, L., and O. Maimon (2005), Clustering Methods, in *Data Mining and Knowledge Discovery Handbook*, pp. 321–
604 352, Springer-Verlag, New York.
- 605 Schwarz, G. (1978), Estimating the Dimension of a Model, *Ann. Stat.*, 6(2), 461–464.
- 606 Voronoi, G. F. (1908), Nouvelles applications des paramètres continus à la théorie de formes quadratiques, *J. für die reine*
607 *und Angew. Math.*, 134, 198–287.
- 608 Wang, Y., G. Ouillon, J. Woessner, D. Sornette, and S. Husen (2013), Automatic reconstruction of fault networks from

609 seismicity catalogs including location uncertainty, *J. Geophys. Res. Solid Earth*, 118(11), 5956–5975,
610 doi:10.1002/2013JB010164.

611 Ward, J. H. J. (1963), Hierarchical Grouping to Optimize an Objective Function, *J. Am. Stat. Assoc.*, 58(301), 236–244.

612 Wesson, R. L., and C. Nicholson (1988), Intermediate-term, pre-earthquake phenomena in California, 1975-1986, and
613 preliminary forecast of seismicity for the next decade, *Pure Appl. Geophys. PAGEOPH*, 126(2–4), 407–446,
614 doi:10.1007/BF00879005.

615 Wilks, S. S. (1938), The Large-Sample Distribution of the Likelihood Ratio for Testing Composite Hypotheses, *Ann. Math.*
616 *Stat.*, 9(1), 60–62.

617 Wollherr, S., A. Gabriel, and P. M. Mai (2019), Landers 1992 “Reloaded”: Integrative Dynamic Earthquake Rupture
618 Modeling, *J. Geophys. Res. Solid Earth*, 124(7), 6666–6702, doi:10.1029/2018JB016355.

619 Yang, W., E. Hauksson, and P. Shearer (2012), Computing a large refined catalog of focal mechanisms for southern
620 California (1981–2010): Temporal stability of the style of faulting, *Bull. Seismol.*

621 Zechar, J. D., and T. H. Jordan (2010), Simple smoothed seismicity earthquake forecasts for Italy, *Ann. Geophys.*, 53(3), 99–
622 105, doi:10.4401/ag-4845.

623

624